Applied Catalysis A: General 458 (2013) 119–129

Contents lists available at SciVerse ScienceDirect

Applied Catalysis A: General

journal homepage: www.elsevier.com/locate/apcata

Conversion of diols by dehydrogenation and dehydration reactions on silica-supported copper catalysts

P.A. Torresi, V.K. Díez, P.J. Luggren, J.I. Di Cosimo*

Catalysis Science and Engineering Research Group (GICIC), INCAPE, UNL-CONICET, Santiago del Estero 2654, 3000 Santa Fe, Argentina

ARTICLE INFO

Article history:
Received 11 March 2013
Accepted 23 March 2013
Available online 29 March 2013

Keywords:
1,3-Butanediol
Dehydration
Dehydrogenation
Copper
Biomass upgrading

ABSTRACT

The gas-phase conversion of a 1,3-polyol (1,3-butanediol) containing primary and secondary OH functions was studied on a series of copper-silica catalysts, *Z*CuSiO$_2$ (Z = 1–25 wt.% Cu), and thoroughly characterized by several techniques such as BET surface area, TPR, XRD, N_2O chemisorption, and UV-vis-DRS. The physicochemical properties of the *Z*CuSiO$_2$ catalysts depended on whether the metal loading was above or below the copper monolayer surface coverage (Z = 13.5 wt.% Cu). Copper species presenting different degrees of interaction with the silica support were detected. At low Z values Cu^0 dispersion was high ($D \approx 40\%$) due to a predominant contribution of nano-sized Cu species (3 nm) which are difficult to reduce, but for Z > 13.5 wt.%, *D* abruptly dropped to 3–8% because of formation of larger tridimensional Cu clustered species (30 nm) that reduced at lower temperatures because of a decreased copper-silica interaction.

On *Z*CuSiO$_2$ catalysts, dehydrogenation of the 1,3-butanediol secondary OH function prevailed over that of the primary one and therefore valuable ketones were the main reaction products. Consecutively to dehydrogenation, dehydration and hydrogenation reactions also took place. Products of the tandem reaction were the β-hydroxy ketone (4-hydroxy-2-butanone), the α,β-unsaturated ketone (methyl vinyl ketone) and the saturated ketone (methyl ethyl ketone). A direct 1,3-butanediol dehydration pathway toward methyl ethyl ketone was also found. Reaction pathways were strongly dependent on the Cu loading and therefore on the kind of Cu species (isolated or clustered). When compared at similar conversion levels, selectivity to the dehydrogenation product 4-hydroxy-2-butanone increased with Z suggesting that on large Cu^0 particles 4-hydroxy-2-butanone was released to the gas phase before being converted in consecutive steps. On the contrary, on highly dispersed Cu^0 crystals of low Cu loading catalysts, 1,3-butanediol was readily dehydrated giving the saturated ketone.

Kinetically relevant reaction steps of 1,3-butanediol conversion by dehydrogenation and dehydration were promoted on Cu^0 sites. Dehydration of the intermediate 4-hydroxy-2-butanone also occurred on Cu^0 sites. Turnover rates were constant on Cu^0 nano particles and slightly higher on clustered species.

1. Introduction

Short chain polyols combining primary and secondary hydroxyl groups are interesting molecules since transformation of one or all the OH groups can lead to valuable compounds used as building blocks. Recently, several processes have attracted much attention because they postulate the production of polyols from renewable sources. In particular, glycerol, a polyol containing one secondary and two primary hydroxyl groups, is nowadays produced in large quantities as the main coproduct of the biodiesel synthesis by oil or fat transesterification. The increasing production of biodiesel around the world offers the opportunity to convert glycerol into value-added chemicals. Glycerol transformation may be oriented toward production of novel compounds or to substitution of existing environmentally unfriendly technology.

One of the most widely studied routes for glycerol transformation is by hydrogenolysis reactions that in turn generate glycols such as 1,2-ethanediol and 1,3- and 1,2-propanediols [1]. These diols are widely used as antifreeze in automobile cooling systems and in the formulation of many compounds [2]. Also butanediols can be synthesized from renewable feedstocks such as glycerol and bioethanol by fermentation [3] or catalytic [4,5] routes.

Biomass-derived polyols such as glycerol and diols present a wide range of potential uses as platform chemicals since they can be converted into valuable products by dehydration, dehydrogenation, or by tandem dehydrogenation-dehydration-hydrogenation reactions leading toward unsaturated alcohols [6,7], furans [8,9], hydroxycarbonyl (aldol) compounds [10–14] and unsaturated carbonyl compounds [15,16], among other products.

* Corresponding author. Tel.: +54 342 4555279; fax: +54 342 4531068.
E-mail address: dicosimo@fiq.unl.edu.ar (J.I. Di Cosimo).

0926-860X/$ – see front matter © 2013 Elsevier B.V. All rights reserved.
http://dx.doi.org/10.1016/j.apcata.2013.03.031

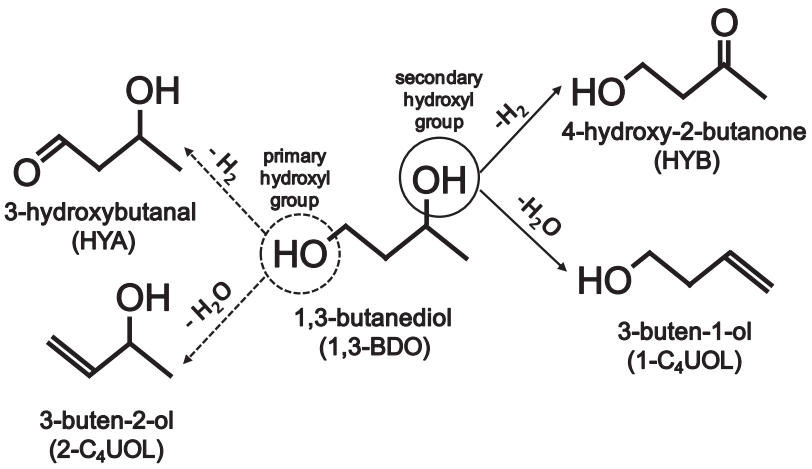

Scheme 1. 1,3-BDO dehydrogenation and dehydration reactions.

In particular, selective dehydrogenation of just one OH group of diols leads to the production of aldol compounds (hydroxyketones or hydroxyaldehydes). The combination of OH and C=O functions in aldol units makes these compounds very attractive [17,18] since they are present in many pharmaceutical formulations and in organic synthesis intermediates.

As an example of all these reactions, 1,3-butanediol (1,3-BDO), a diol containing one primary and one secondary hydroxyl group, can undergo dehydrogenation and dehydration reactions, as depicted in Scheme 1, giving valuable aldol products and unsaturated alcohols used in the pharmaceutical and polymer industry, respectively. Furthermore, tandem 1,3-BDO dehydrogenation-dehydration-hydrogenation gives a β-hydroxy ketone (4-hydroxy-2-butanone, HYB) and a α,β-unsaturated ketone (methyl vinyl ketone, MVK), which are important intermediates for the synthesis of food formulations [19], pesticides, terpenoids as well as steroids, anticancer and other medical drugs [18,20], and also a saturated ketone (methyl ethyl ketone, MEK) with many applications as a solvent in the resin industry.

The 1,3-BDO transformation, by dehydrogenation and consecutive reactions, has been investigated under a variety of reaction conditions by enzymatic catalysis [18,21], homogeneously and heterogeneously catalyzed oxidation [19,22], and gas-phase heterogeneous catalysis [13,14], thereby obtaining a diversity of products.

In this work we present our investigations on the gas-phase conversion of 1,3-BDO on copper-silica catalysts prepared by ion exchange. The aim of this work was to develop a catalytic process capable of operating in a continuous reaction system under atmospheric pressure and without solvent, to selectively dehydrogenate the secondary hydroxyl of 1,3-BDO as the first reaction step. Thus, the reaction was oriented toward formation of HYB, MVK and MEK. Copper-based catalysts were chosen due to the known properties of this metal to preferentially activate the O—H bond of alcohols, giving aldehydes and ketones by dehydrogenation at mild temperatures without significantly breaking the C—C and C—O bonds [23]. A systematic investigation was undertaken to prepare and characterize a series of copper-silica catalysts with different metal loadings to use them to promote the reaction. Several techniques were used such as N_2 adsorption, TPR, XRD, N_2O chemisorption, and UV–vis–DRS, with emphasis on the assessment of the metal reducibility and dispersion and metal-silica degree of interaction.

Results show a strong effect of the copper content on the physicochemical properties and on the catalytic performance of these materials. The 1,3-BDO transformation occurs by parallel dehydrogenation and dehydration reactions or by a consecutive dehydrogenation-dehydration-hydrogenation reaction sequence depending on the copper loading. Also, distinct selectivity values were obtained depending on the metal concentration range below or above the copper loading for complete monolayer surface coverage, suggesting a shift of the reaction pathway from dehydration to dehydrogenation reactions as the metal loading increases. Moreover, participation of surface silica or copper species (Cu^0 or Cu^{2+}) in the catalytic cycle was studied. Promotion of dehydration and dehydrogenation steps on Cu^0 sites was confirmed by the linear increase of the reaction rate with the Cu^0 surface area.

2. Experimental

2.1. Catalyst synthesis and activation

Silica-supported copper catalysts with metal loading between 1.0 and 25.0 wt.% were prepared by ion exchange through the so called "chemisorption-hydrolysis" technique (CH) [24,25]. To facilitate sample handling, the silica support (Evonik Aerosil 380, $380 \pm 30\ m^2/g$) was used after wetting with distilled water and drying at 373 K. A concentrated solution of NH_4OH was added to an aqueous solution of $Cu(NO_3)_2{\cdot}3H_2O$ (Anedra) containing the required Cu concentration in order to generate a $[Cu(NH_3)_4(H_2O)_2]^{2+}$ complex at a pH of 9. 5 g of dry support were contacted with 25 mL of the complex-containing solution. Then, the mixture was slowly diluted to 2.0 L under stirring using distilled water. Solids were separated by vacuum filtration and then washed with distilled water and dried overnight at 363 K. After that, samples were sieved to retain particles between 180 and 480 μm. Finally, solids were calcined in air at 623 K during 5 h. The resulting Cu-doped SiO_2 samples were denoted as ZCuSiO$_2$, where Z is the Cu content expressed in wt.%.

2.2. Catalyst characterization

The chemical content of Cu in ZCuSiO$_2$ catalysts was analyzed by Atomic Absorption Spectrometry (AAS). BET surface areas (SA) were measured by N_2 physisorption at its boiling point using an Autosorb Quantachrome 1-C sorptometer and mean pore sizes ($\bar{r}$) were calculated using the Wheeler's equation ($\bar{r} = 2Vg/SA$, where Vg is the pore volume). The structural properties of solid samples were determined by X-ray diffraction (XRD) technique using a Shimadzu XD-D1 instrument.

The dispersion of the metallic copper particles (D), defined as the ratio of the number of surface metallic copper atoms (Cu^S) to the total copper atoms (Cu^T) in the catalyst formulation, was

determined by two consecutive experiments of temperature programmed reduction (TPR), using a reducing mixture of 5% H_2/Ar at a flow rate of 50 cm^3/min and loading the reactor with the same molar amount of copper (150 μmol) in each experiment. Heating rates of 10 K/min from 298 to typically 653 K were used. A mass spectrometer (MS) in a Baltzers Omnistar unit monitored the hydrogen consumption. Quantitative H_2-uptakes were calculated by integration of the two experimental TPR curves and using previous calibration with CuO powder (Cicarelli, PA). The first TPR experiment was performed after the oxidation of the catalyst total copper atoms to CuO in flowing air (50 cm^3/min) at 623 K. Thus, from this TPR experiment the Cu^T value was obtained. A consecutive second TPR experiment was carried out after re-oxidation of the surface copper metal atoms to Cu_2O using N_2O and a stoichiometry of $Cu^S/N_2O = 2$. Sample was exposed to pulses of N_2O at 363 K until surface saturation. The Cu:H_2 stoichiometry involved in each TPR experiment was used to calculate the Cu dispersion as $D = Cu^S/Cu^T = 2A^S/A^T$, where A^S and A^T are the areas corresponding to the H_2 uptake of the second and first TPR, respectively [26,27]. The average copper particle size was determined as $L\,(nm) = 1.04/D$ assuming a Cu surface density of 1.47×10^{19} Cu atoms/m^2 [28] and spherical Cu crystallites [29]. Then, with the surface density and D values, the Cu^0 specific surface area was calculated as A_{Cu} (m^2/g cat) = $6.44\,D \times Z$.

UV–vis–DRS spectra of the $ZCuSiO_2$ samples were recorded using an OL Series 750 Automated Spectroradiometric Measurement System spectrophotometer with a diffuse reflectance chamber and a 150 mm diameter integrating sphere with internal polytetrafluoroethylene (PTFE) coating. Samples were compacted in a sample holder to obtain a sample thickness of ≈2 mm; the spectra were then recorded in the reflectance mode (R) at room temperature in the range 200–800 nm and converted to the Kubelka–Munk function: $f(R_\infty) = (1 - R_\infty)^2/2R_\infty = KC$, where K is a constant that includes the sample scattering coefficient and absorptivity, and C is the analyte concentration [30]. PTFE was used as the reference material.

The chemical nature of surface acid sites was determined by Infrared Spectroscopy (IR) of pyridine using a Shimadzu FTIR Prestige-21 spectrophotometer. Experiments were carried out using an inverted T-shaped cell containing the sample wafer and fitted with CaF_2 windows. The absorbance scales were normalized to 20-mg wafers. Sample wafers were evacuated at 623 K, then cooled down to room temperature to take the catalyst spectrum. After exposure to 0.12 kPa of pyridine at room temperature samples were evacuated consecutively at 298, 373, 423 and 473 K and the resulting spectrum at each evacuation temperature was recorded at room temperature. Spectra of the adsorbed species were obtained by subtracting the catalyst spectrum.

2.3. Catalytic testing.

Vapor-phase conversion of 1,3-butanediol (1,3-BDO) was carried out at 523 K and 101.3 kPa in a fixed-bed reactor at contact times (W/F^0_{BDO}) of 0.05–1.2 g cat h/mol of 1,3-butanediol, which correspond to gas hourly space velocity values (GHSV) between 14.7 and 92.3 h^{-1}. Before the catalytic tests catalysts were pretreated in a flow of N_2 at 623 K for 1 h in order to remove water and carbon dioxide. Then, catalysts were reduced in situ in flowing H_2 (35 cm^3/min) at 573 K for 1 h. 1,3-BDO (Aldrich GC, 99.0% purity) was introduced via a syringe pump and vaporized into flowing N_2 (150 cm^3/min) to give a 1,3-BDO partial pressure of 2.3 kPa. Reaction products were analyzed by on-line gas chromatography using an Agilent 7890A chromatograph equipped with flame ionization detector and a 0.2% Carbowax 1500/80–100 Carbopack C packed column. Data were collected every 0.5 h for 5 h. Main reaction products were identified as 4-hydroxy-2-butanone (HYB), methyl ethyl ketone (MEK), methyl vinyl ketone (MVK). Minor amounts of acetaldehyde (C_2AL), methanol (C_1OL), ethanol (C_2OL) and acetone (C_3K) were also quantified. HYB conversion experiments were performed in a similar fashion at 523 K and $W/F^0_{HYB} = 2.92$ g cat h/mol and at a HYB (Sigma Aldrich, 95%) partial pressure of 0.9 kPa. Turnover (TOR) rates (for reactants) are defined as the moles of reactant converted per mol surface site and per second in the reactor. Additional catalytic tests were carried out for both, 1,3-BDO and HYB conversion reactions on pure CuO and SiO_2. Site-time yields (STY) for each product were similarly calculated as the moles of reactant converted to a given product per mol surface site and per second. Due to a slight catalyst deactivation process, the catalytic results reported here were calculated by extrapolation of the reactant and product concentration curves to zero time on stream. Then, X, Y and S represent conversion, yield and selectivity at $t = 0$, respectively.

3. Results and discussion

3.1. Chemical, textural and structural properties of $ZCuSiO_2$ catalysts

The basic pH used during catalyst preparation by the chemisorption-hydrolysis (CH) method allows the formation of a $[Cu(NH_3)_4(H_2O)_2]^{2+}$ complex and charges negatively the solid surface by removing surface protons from silica silanols and therefore generating the exchange sites. The following hydrolysis of the complex causes the deposition of finely dispersed exchanged copper species [24].

The chemical, textural and structural properties of the $ZCuSiO_2$ catalysts after calcination at 623 K are presented in Table 1. The Cu loading was varied in the range of 1.1–25.0 wt.%, i.e., in a compositional range much wider than the 6–9 wt.% previously reported for the CH method [25]. The calculations of the Cu monolayer coverage fraction, f, (Table 1, column 6) were carried out considering that the exchanged copper species has the size of the octahedral $[Cu(NH_3)_4(H_2O)_2]^{2+}$ complex with elongated tetragonal distortion [31] (23.4 $Å^2$, calculated with the ACD/ChemSketch 11.0 package). The results indicate that the SiO_2 surface may be already covered by one monolayer of the Cu complex ($f = 1$) at about 13.5 wt.% Cu loading. On the other hand, the silica exchange capacity calculated using a stoichiometry of Cu^{2+}:silanol = 1:2 [32] and a silanol surface density of 5×10^{18} OH/m^2 for hydrated silica [33], gave 9 wt.% Cu, a value reasonably close to the number we calculated from the Cu complex size.

Since we attempted to prepare some catalysts with copper contents that largely exceed the silica exchange capacity (13.5 wt.%) and according to the AAS analyses of Table 1 Cu loadings above 13.5 wt.% were indeed obtained, it seems that at these high Cu contents and before calcination, in addition to the exchanged species, Cu^{2+} ions were probably retained on the surface as finely dispersed copper nitrate hydroxide, copper hydroxide, or other species whose appropriateness has been debated in the literature for other ion exchange methods [31,34] and goes beyond the scope of this work. Thus, at Cu contents above 10–14 wt.%, the silica surface would be covered by the exchanged complex and stacked layers of deposited species that after calcination are expected to form tridimensional CuO species on SiO_2. In agreement with these calculations, the color of the calcined $ZCuSiO_2$ samples was light greenish-blue up to 11.9 wt.% Cu and dark greenish-brown at higher loadings as expected in CuO-containing samples, Table 1.

Elemental analysis revealed that for Cu loadings between 1.1 and 11.9 wt.% ($f < 1$) the preparation method gave quantitative results but for higher Cu loadings the measured Z values were lower than the nominal ones. This fact suggested that when dealing with

Table 1
Physicochemical properties of $ZCuSiO_2$ catalysts.

Catalyst	Cu loading, Z		Color[b]	SA [c] (m^2/g)	Mean pore size[d] (Å)	Monolayer coverage fraction, f [e] (m^2 Cu in the complex/m^2 SiO_2)	XRD analysis	UV–vis–DRS analysis		
	Nominal (wt.%)	By AAS (wt.%)					Phases detected	Peak area (%)		
								A_I	A_O	A_T
SiO_2[a]	–	–	White	341	–	–	SiO_2	–	–	–
$1.1CuSiO_2$	1.0	1.1	Light bluish-white	256	89	0.07	SiO_2	48.3	37.3	14.3
$2.6CuSiO_2$	3.0	2.6	Light bluish-white	279	95	0.17	SiO_2	–	–	–
$5.6CuSiO_2$	6.0	5.6	Light greenish-blue	241	91	0.39	SiO_2	24.8	39.8	35.2
$8.5CuSiO_2$	8.0	8.5	Light greenish-blue	225	91	0.60	SiO_2	24.8	40.3	34.8
$11.9CuSiO_2$	13.0	11.9	Light greenish-blue	224	107	0.88	SiO_2	18.4	42.0	39.4
$15.6CuSiO_2$	17.0	15.6	Dark brownish-green	216	136	1.20	CuO + SiO_2	–	–	–
$25.0CuSiO_2$	35.0	25.0	Dark greenish-brown	215	–	2.17	CuO + SiO_2	n/q[f]	n/q[f]	n/q[f]

[a] After wetting with water and drying at 373 K.
[b] Calcined samples.
[c] BET surface area.
[d] By the Wheeler's equation.
[e] f = 1 at 13.5 wt.% Cu.
[f] Not quantified.

the concentrated solutions of the copper complex needed to reach high Z values ($f > 1$), there was not enough activated silica surface sites where to exchange the complex and that deposition of the remaining Cu^{2+} ions in the solution was not complete.

The $ZCuSiO_2$ catalysts presented high surface areas (SA) in the range of 215–279 m^2/g but the SA values gradually decreased with increasing the Cu loading. This SA decrease is accompanied by an increase of the mean pore size, probably reflecting the silica pore blocking due to formation of large CuO crystallites at high Cu loadings, as will be discussed later.

The calcined $ZCuSiO_2$ catalysts were analyzed by XRD. All samples showed a broad signal at around 22° corresponding to amorphous silica. For copper contents of up to 11.9 wt.% ($f < 1$) no crystalline copper phase was observed indicating formation of small CuO domains highly dispersed on the SiO_2 surface and non detectable by XRD. In agreement with the calculations of the Cu fractional surface coverage at higher copper loadings ($f > 1$), samples $15.6CuSiO_2$ and $25.0CuSiO_2$ presented a CuO phase (tenorite). Crystallinity calculations on the CuO diffraction lines showed an increase in sample $25.0CuSiO_2$ compared to $15.6CuSiO_2$ which is consistent with a higher crystallite size attributed to particle agglomeration.

3.2. Copper species in $ZCuSiO_2$ catalysts. Reducibility and Cu^0 dispersion

The reducibility of Cu species in $ZCuSiO_2$ samples was investigated by TPR. Fig. 1 shows the reduction profiles obtained for $ZCuSiO_2$ calcined at 623 K; CuO was also included as reference. The $ZCuSiO_2$ samples reduced completely below 600 K giving a single broad peak at 450–550 K. No hydrogen evolution was detected above 600 K as shown in Fig. 1 for sample $8.5CuSiO_2$. Complete reduction in a similar temperature range has been also reported by others for low-loading silica-supported copper samples prepared by the CH method [35]. Reduction of the totality of the copper atoms in the sample was confirmed by previous quantitative calibration with CuO and considering that the observed peaks of Fig. 1 correspond to $Cu^{2+} \rightarrow Cu^0$ reduction [36]. The temperature at the peak maximum (T_M) shifted to lower values as the Cu loading increased suggesting the generation of more reducible species because of a weaker copper crystallites-silica support interaction. Thus, the T_M values gradually approached that of the reference bulk CuO (Table 2).

Copper dispersion (D) in $ZCuSiO_2$ catalysts was investigated by combining TPR and N_2O chemisorption experiments in a two-step procedure as described in Section 2.2. The second TPR experiment was carried out after re-oxidation of surface copper atoms to Cu_2O by adsorptive decomposition of N_2O at 363 K. Surface re-oxidation led to more reducible species as indicated by the lower reduction temperatures of the second TPR (not shown) compared to the first

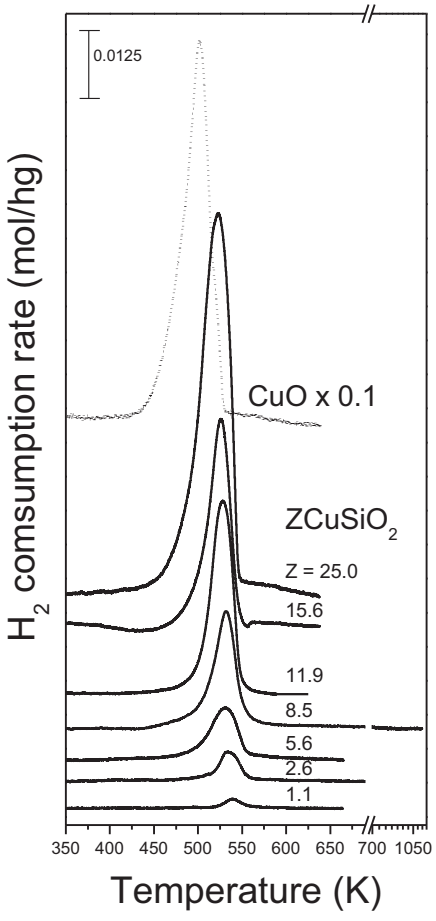

Fig. 1. TPR profiles of $ZCuSiO_2$ and CuO catalysts.

Table 2
Reducibility and dispersion of Cu in $ZCuSiO_2$ catalysts and 1,3-BDO reaction data.

Catalyst	Cu^0 dispersion, D [a] (%)	Cu^0 crystallite size, L [b] (nm)	T_M [c] (K)	TOR[d] (1/s)	E_a [f] (kcal/mol)
$1.1CuSiO_2$	36.6	2.8	539	1.36	
$2.6CuSiO_2$	32.0	3.2	535	1.17	
$5.6CuSiO_2$	27.2	3.8	532	1.27	8.4
$8.5CuSiO_2$	27.5	3.8	532	1.15	
$11.9CuSiO_2$	25.3	4.1	527	1.15	
$15.6CuSiO_2$	7.8	13.3	525	1.76	
$25.0CuSiO_2$	3.4	30.6	522	1.84	6.9
CuO	<1.0[e]	–	502	–	

[a] By N_2O titration.
[b] Calculated from D.
[c] Temperature at peak maximum from TPR (Fig. 1).
[d] Mol 1,3-BDO/s mol surface Cu, $T = 523$ K, $\bar{P}_{BDO} = 2.33$ kPa.
[e] Below detection limit
[f] Apparent activation energy at 493–533 K.

one. Similar findings were reported by Fierro et al. for reoxidation of Cu-Zn catalysts with CO_2 [37]. By integration of both TPR profiles the D values were calculated (Table 2). Silica-supported catalysts with Cu dispersions of up to 37% were obtained for low metal loadings (sample $1.1CuSiO_2$). However, the D values slightly decreased at increasing Cu loadings reaching a value of 25% for sample $11.9CuSiO_2$. The Cu^0 crystallite size (L) concomitantly increased from 2.8 to 4.1 nm, Table 2. Above the Cu loading for monolayer surface coverage (samples $15.6CuSiO_2$ and $25.0CuSiO_2$), Cu dispersion drastically decreased to 3–8%, reflecting formation of large Cu^0 crystallites of 13.3–30.6 nm.

The presence of surface copper species with different degrees of interaction with the silica support, that are responsible for sample color, reducibility and metal dispersion changes depending on the Cu loading, was confirmed by UV–vis-DRS of selected calcined $ZCuSiO_2$ samples (Fig. 2). Three copper species with different chemical environments were detected in the spectra of low and high Cu loading $ZCuSiO_2$ samples. Similar spectra were previously reported for other silica-supported copper samples prepared by different techniques [24,35,38]. No band assignment could be performed in the spectrum of sample $25.0CuSiO_2$ since the reflectance values were lower than 10% due to the dark sample color.

The maximum in UV–vis–DRS spectra at about 235–250 nm was attributed to O^{2-} to Cu^{2+} ligand to metal charge-transfer in mononuclear (isolated) species [35]. As the Cu content increased, a shoulder at about 290–350 nm developed, this band being assigned to the charge transfer between Cu^{2+} and oxygen in oligonuclear $[Cu–O–Cu]_n$ surface species [35,38,39] probably forming nano-sized patches. Another effect of the increasing Cu loading was the developing of an intense and broad band at about 700 nm, which is typical of copper in tridimensional or clustered CuO species [40]. Isolated and oligonuclear species derive from exchanged Cu^{2+} ions [35] whereas in the formation of clustered species (band at 700 nm) the contribution of deposited species has to be taken into account.

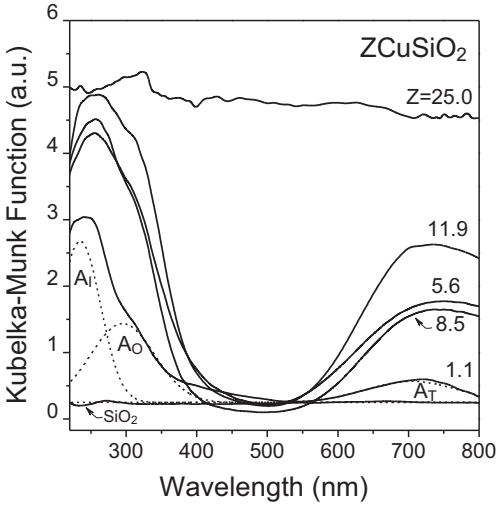

Fig. 2. UV–vis–DRS spectra of selected $ZCuSiO_2$ catalysts and reference SiO_2 [A_I: isolated, A_O: oligonuclear, and A_T: tridimensional copper species].

The experimental spectra of these samples were deconvoluted as three Gaussian bands as shown in dotted lines for sample $1.1CuSiO_2$ in Fig. 2. Assuming that the Kubelka–Munk theory applies to the $ZCuSiO_2$ samples, the Kubelka–Munk function linearly relates the copper species concentration with the band intensity [30]. Thus, the areas under the Gaussian curves of Fig. 2 are a measure of each copper species concentration provided that the scattering coefficient and absorptivity are similar for the three species. Table 1 shows the quantitative results after deconvolution, where A_I, A_O and A_T denote the peak area % of isolated, oligonuclear and tridimensional copper species, respectively. Clearly, at low Cu loadings isolated and oligomeric Cu^{2+}-silica O^{2-} species predominated, suggesting that at those loadings the preparation method generates well dispersed ion exchanged Cu^{2+} species that strongly interact with the oxygen ions of the silica support, therefore explaining the high dispersion values and high reduction temperatures observed for these samples in Fig. 1 and Table 2. On the contrary, the UV–vis–DRS results of Table 1 indicate that copper loadings approaching the monolayer surface coverage ($f = 0.88$, sample $11.9CuSiO_2$) enhanced the contribution of small tridimensional domains of CuO species not yet detectable by XRD. At even higher loadings ($f > 1$, samples $15.6CuSiO_2$ and $25.0CuSiO_2$) the catalyst surface was covered by large CuO particles from deposited copper species which reduce at lower temperatures, Table 2.

3.3. Reaction pathways for 1,3-butanediol conversion

On $ZCuSiO_2$ catalysts, we investigated the reaction pathways of the gas phase 1,3-BDO conversion. Regardless of the reaction conditions and catalyst composition, the 1,3-BDO dehydration products (unsaturated alcohols) postulated in Scheme 1 were observed only in negligible amounts on reduced $ZCuSiO_2$ samples. To further investigate the 1,3-BDO conversion by dehydrogenation and dehydration and the existence of consecutive reactions, several catalytic tests varying the contact time (W/F^0_{BDO}) were performed at typical reaction conditions with samples $5.6CuSiO_2$ and $25.0CuSiO_2$ representing respectively, low and high Cu loading catalysts.

Fig. 3 shows the 1,3-BDO conversion (X_{BDO}) and the main product yields (Y_j) plotted as a function of W/F^0_{BDO}. The local slope of

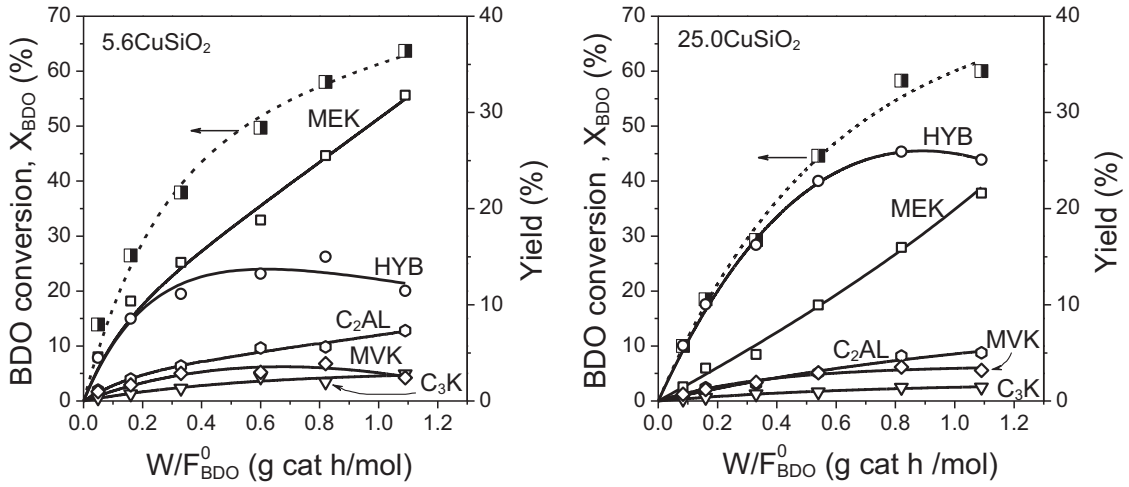

Fig. 3. 1,3-BDO conversion and product yields on $5.6CuSiO_2$ and $25.0CuSiO_2$ as a function of contact time (W/F^0_{BDO}) [T = 523 K, $\bar{P}_{BDO}$ = 2.33 kPa, t = 0].

the curves is either the 1,3-BDO conversion rate (r_{BDO}) or the product formation rate (r_j) at a given X_{BDO} and W/F^0_{BDO} value. Each data point represents a catalytic run with a fresh catalyst load. In order to prevent our analysis from being influenced by the slight deactivation process, the results of Fig. 3 were obtained at t = 0 as described in Section 2.3. Like the reactant, main reaction products contained 4 carbon atoms; they were the 1,3-BDO dehydrogenation product (HYB), the saturated ketone (MEK) and the α,β-unsaturated ketone (MVK). The C_4 compounds accounted in all cases for ≈80% of the products.

As shown in Scheme 1, 1,3-BDO dehydrogenation might occur at the primary as well as the secondary OH group giving a hydroxyaldehyde (3-hydroxybutanal, HYA) or a hydroxyketone (4-hydroxy-2-butanone, HYB), respectively.

Hydroxycarbonyl compounds such as HYB and HYA tend to further react at the conditions of the gas phase reaction giving different products. For instance, in previous work on aldol condensation reactions toward C_6 compounds, we hardly detected the intermediate hydroxyketone since it rapidly dehydrated and hydrogenated toward the saturated ketone on a bifunctional copper/acid-base catalyst [23]. Thus, the saturated (MEK) and the α,β-unsaturated (MVK) ketones detected here among the reaction products suggest that in addition to the initially formed dehydrogenation products (HYB and HYA), consecutive dehydration and hydrogenation reactions might take place, Scheme 2. HYA was never observed at any reaction conditions on the $ZCuSiO_2$ samples, in contrast to HYB that was always one of the main reaction products. This result indicates that the main 1,3-BDO dehydrogenation route involves the secondary OH group, in agreement with previous reports showing that secondary alcohols are better hydrogen donors than the primary ones [41,42]. However, formation of HYA in low concentration can be inferred from formation of minor compounds.

The nonzero initial slope of the HYB curve, i.e., at $W/F^0_{BDO} \approx 0$ is consistent with direct formation from 1,3-BDO; for products consecutively formed from HYB, the initial slopes are expected to be zero. However, for sample $25.0CuSiO_2$, the initial slopes of Y_{MEK} and Y_{MVK} curves are not zero but smaller compared to that of Y_{HYB} thereby suggesting a fast dehydration of HYB into MVK that takes place at contact times much shorter than those used in our experiments of Fig. 3. Furthermore, the higher initial slope of the Y_{MEK} curve compared to that of Y_{MVK} is inconsistent with MEK formation in a consecutive step from MVK. Thus, for the reaction pathways of Scheme 2 we have to take into account the contribution of a direct pathway toward MEK formation from 1,3-BDO, which would explain the slopes. This effect is even more noteworthy in the results of sample $5.6CuSiO_2$ in Fig. 3 where the initial slopes of the Y_{MEK} and Y_{HYB} curves are similar indicating that the direct dehydration pathway toward MEK is enhanced on low copper loading samples. MVK on the other hand, was always obtained in low concentration regardless of the catalyst composition and contact time due to the high reactivity of α,β-unsaturated ketones at our reaction temperatures.

Results of Fig. 3 show that for similar contact time and conversion range, low and high copper loading samples presented distinctive performances for 1,3-BDO dehydration, dehydrogenation and successive reactions and therefore, the product distribution was significantly different. Whereas at high conversions the dehydrogenation product HYB was the main product on catalyst $25.0CuSiO_2$, MEK formation by mainly direct dehydration of 1,3-BDO predominated on sample $5.6CuSiO_2$.

Small amounts of short chain compounds such as C_1OL, C_2OL, C_3K, C_1AL and C_2AL that add up less than 15% selectivity were also detected among several minor unidentified products. The presence of reaction products with less carbon atoms than the reactant suggests that besides being converted through the dehydration-hydrogenation conversion route, the intermediate hydroxycarbonyl compounds (HYB and HYA) might decompose by C—C bond cleavage reactions such as retroaldol-like reactions [14], giving aldehydes, ketones and alcohols as depicted in Scheme 2. Thus, the formation of small amounts of C_2AL and C_2OL is explained by decomposition of the unstable HYA (not detectable in the reaction products), whereas that of C_3K and C_1OL is assigned to decomposition of HYB by similar reactions.

The selectivity ratio between decomposition and C_4 products formed from HYB, $(C_3K + C_1OL)/(MVK + MEK)$, was about 0.1 for low and high Cu loading samples indicating that the dehydration-hydrogenation pathway predominates over the C—C bond breaking route for transformation of HYB. Contrarily, the dehydration-hydrogenation products formed from HYA (C_4UAL, C_4AL and C_4OL) were observed in negligible amounts compared to the decomposition products (C_2AL and C_2OL). These differences in the dehydration extent between the secondary (HYA) and the primary (HYB) hydroxyl group of hydroxycarbonyl compounds cannot be interpreted in terms of catalyst acidic properties since on an acid catalyst the former is supposed to dehydrate more easily than the latter [43]. One explanation is the fact that dehydration of HYA leads to an unsaturated aldehyde (C_4UAL) whereas that of HYB forms

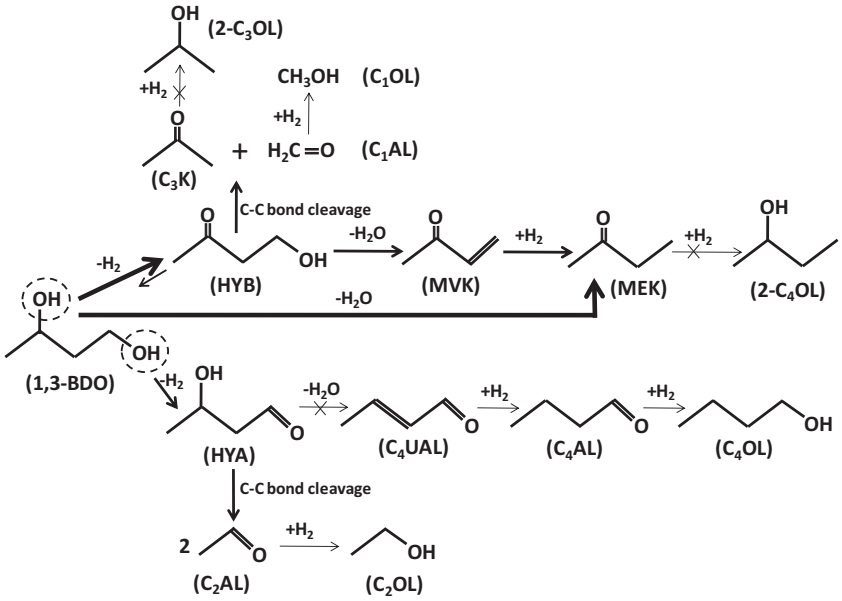

Scheme 2. Reaction scheme for 1,3-BDO conversion on ZCuSiO$_2$ catalysts.

an unsaturated ketone (MVK). Unsaturated aldehydes are less stable than unsaturated ketones and therefore HYA decomposition by retroaldolization giving a single product, C_2AL, would be favored compared to dehydration.

Regarding hydrogenation of carbonyl compounds, the presence of negligible amounts of 2-C_4OL and 2-C_3OL compared to C_2OL and C_1OL, confirms that the ketone carbonyl group is more difficult to reduce than that of aldehydes (Scheme 2), because aldehydes have lower reduction potentials than dialkyl ketones [41].

Scheme 2 summarizes the reaction network for 1,3-BDO conversion on ZCuSiO$_2$ catalysts, where the thickness of the arrow lines indicates the relative importance of the reactions and emphasizes that the main reaction products arise from activation of the secondary OH group of 1,3-BDO either by dehydration or dehydrogenation.

3.4. Effect of the copper content on the catalytic performance. Active site identification

The effect of the Cu loading on the catalytic performance of the ZCuSiO$_2$ samples was studied by testing the different catalysts under similar reaction conditions. Previously, a blank test using pure SiO$_2$ confirmed that the support was inactive for performing the 1,3-BDO dehydration or dehydrogenation reactions shown in Scheme 1.

The formation and conversion rates for products (r_j) and reactant (r_{BDO}) were calculated for the different ZCuSiO$_2$ samples. Fig. 4a shows the r_{BDO} and the Cu^0 specific surface area (A_{Cu}) values calculated from N_2O decomposition as a function of the Cu loading (Z). The linear dependence of A_{Cu} up to a loading of 11.9 wt.% reflects the fact that the L values (Table 2) varied slightly (2.8–4.1 nm) for Cu

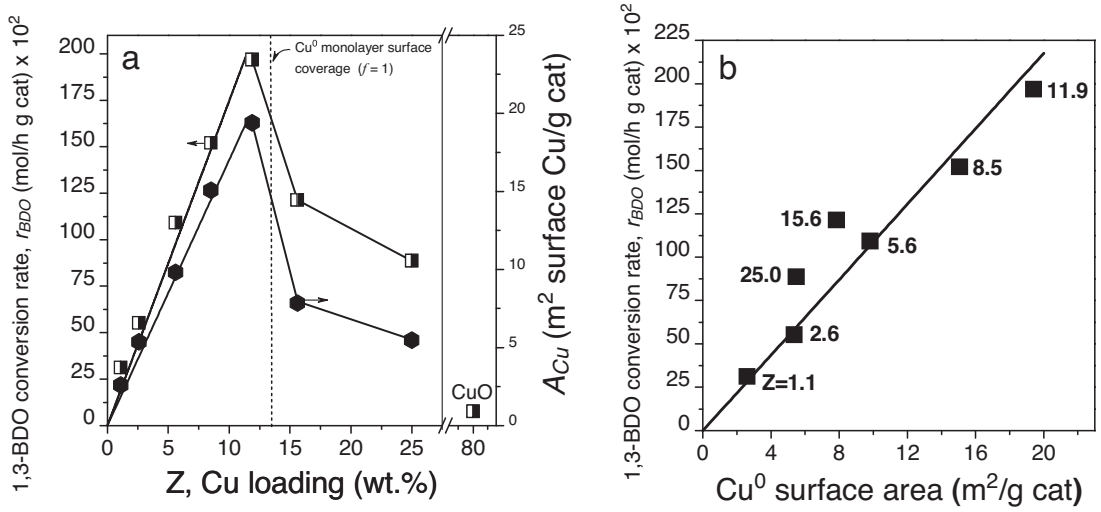

Fig. 4. (a): 1,3-BDO conversion rate (r_{BDO}) and Cu^0 surface area (A_{Cu}) on ZCuSiO$_2$ catalysts as a function of the Cu content. CuO activity also included; (b): linear dependence between 1,3-BDO conversion rate (r_{BDO}) and Cu^0 surface area [T = 523 K, $\tilde{P}_{BDO}$ = 2.33 kPa, t = 0, A_{Cu}: see Section 2.2].

loadings below the monolayer surface coverage and therefore, A_{Cu} increased almost proportionally to Z. Formation of much larger Cu^0 crystallites at higher loadings caused the abrupt drop of A_{Cu}. The highest A_{Cu} (19.4 m^2/g cat), measured for sample 11.9$CuSiO_2$, is a value typical of those reported in the literature (9–33 m^2/g cat) for 8–10 wt.% copper catalysts prepared by ion exchange techniques [24,44]. The A_{Cu} value for the reference CuO sample could not be measured because the metal dispersion was below the detection limit of the technique (~1%). Thus, the metallic particles of the CuO sample after reduction are much larger than those of the Z$CuSiO_2$ catalysts.

From the analogous volcano-shaped curves of Fig. 4a for activity and Cu^0 specific surface area as a function of Z, a linear correlation (Fig. 4b) was obtained between r_{BDO} and A_{Cu}, thereby suggesting that kinetically relevant steps in the 1,3-BDO conversion pathways by dehydration and dehydrogenation are promoted on Cu^0 surface sites. It has been reported before that the conversion rate of other polyols follows a similar linear dependence, such as the gas phase tandem dehydration-hydrogenation of glycerol on Cu-SiO_2 catalysts with Cu^0 surface areas in the range of 1–4 m^2/g cat [45].

Thus, in Fig. 4a, the total activity, r_{BDO}, increased linearly with Z for Cu loadings below the monolayer surface coverage as more Cu^0 species became available in this compositional range in which mostly isolated and oligonuclear ion exchanged copper species predominate (Table 1). At higher loadings, formation of large tridimensional Cu^0 particles, in which Cu^0 species became less accessible, decreased the total activity per g catalyst; confirming this trend, the activity of a commercial CuO sample with much larger particles was much lower (0.076 mol/h gcat, Fig. 4a).

As expected from the linear relationship between r_{BDO} and exposed Cu^0 species, constant turnover rate (TOR) values were calculated, Table 2, which confirm that 1,3-BDO conversion indeed occurs on Cu^0 species. Furthermore, a variation in Cu^0 particle size between 2.8 and 4.1 nm did not affect the reactivity in terms of TOR values. The TOR values on bigger particles are larger by less than a factor of 2 compared to the values on nano particles. These slight differences are not relevant and might be the consequence of experimental uncertainties in measuring the surface area at high loadings. Calculations of the apparent activation energy (E_a) for the overall 1,3-BDO conversion (Table 2) seem to go in the same direction since the E_a value for sample 5.6$CuSiO_2$ (3.8 nm) was quite similar to that for sample 25.0$CuSiO_2$ (30.6 nm).

Sato et al. [10] postulated the dehydrogenation and dehydration of polyols such as 1,2-propanediol and glycerol by homolytic O—H, C—H and C—OH bond dissociations on metallic sites of bifunctional catalysts. In a similar fashion, and from the results of Figs. 3 and 4, we postulate in Schemes 3 and 4 the surface reaction mechanisms of 1,3-BDO conversion on Cu^0 sites. Scheme 3 shows a tandem dehydrogenation-dehydration-hydrogenation route leading toward HYB and MEK. Direct 1,3-BDO dehydration, Scheme 4, involves formation of the unstable unsaturated alcohol 2-C_4UOL which is isomerized to the more stable MEK, as frequently found on metal catalysts [46]. Both the tandem dehydrogenation-dehydration-hydrogenation and direct dehydration reactions begin by surface alcoxide formation after O—H bond breaking at the secondary OH group of 1,3-BDO, and continue with the activation of several C—H bonds and of the C—OH bond at the primary hydroxyl group.

As anticipated in Fig. 3, the distribution of main products was affected by the Cu loading. In order to study in more detail the effect of copper content we present in Fig. 5 the metal particle size as well as the main product selectivity at $t = 0$ and $X_{BDO} \approx 30\%$ as a function of Z for all the Z$CuSiO_2$ samples; selectivity on pure CuO was included as a reference. The conversion level for this study was chosen so that to allow the tandem dehydrogenation–dehydration–hydrogenation sequence

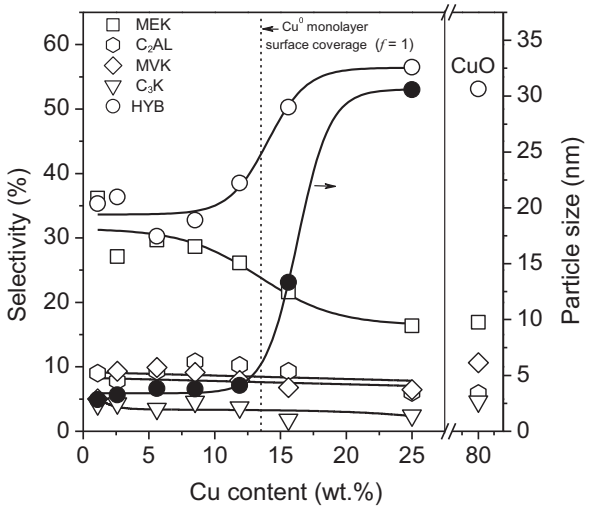

Fig. 5. Product selectivities and Cu^0 particle size on Z$CuSiO_2$ catalysts as a function of the Cu content. CuO selectivity also included [$T = 523$ K, $P_{BDO} = 2.33$ kPa, $t = 0$, $X_{BDO} \approx 30\%$].

to proceed to certain extent. Fig. 5 shows that the selectivities of the major products, HYB and MEK, were similar to each other and slightly varied with Z at Cu loadings below the monolayer surface coverage ($f < 1$). Thus, in parallel to the TOR values of Table 2, the product distribution was not significantly influenced by a Cu^0 particle size change between 2.8 and 4.1 nm. On the contrary, at higher Z values ($f > 1$) S_{HYB} increased and more than tripled the value of S_{MEK}, whereas the metal particles enlarged by a factor of eight. Therefore, at high Cu loadings, whereas direct 1,3-BDO dehydration to MEK seems not to be favored, HYB is released to the gas phase before consecutive dehydration-hydrogenation reactions take place, yielding HYB in high selectivity. A similar effect was quantified on the much larger Cu^0 crystals of pure CuO. Then, the results suggest that S_{HYB} is enhanced on large Cu^0 particles because of a weaker HYB adsorption and a lower catalyst ability to dehydrate both 1,3-BDO and HYB.

Selectivity to MVK, the product formed by HYB dehydration, was always low and almost independent of Z (Fig. 5) and of W/F^0_{BDO} (from Fig. 3). In previous work [47] we reported that Cu^0 surface atoms selectively reduce the C=C bond of α,β-unsaturated ketones yielding the saturated ketone whereas reduction of the C=O bond was thermodynamically unfavored at the conditions of the gas-phase reaction. Here, in light of our previous results, the α,β-unsaturated ketone, MVK, would be an intermediate formed readily from HYB dehydration that converts into MEK by fast consecutive reduction of the C=C bond with surface hydrogen fragments remaining from 1,3-BDO dehydrogenation on Cu^0 surface sites, as shown in step 5 of Scheme 3.

Selectivities to minor products C_2AL and C_3K were low and remained almost unchanged in the entire compositional range. Recently, Sad et al. [48] showed how gas-phase aldol-type C-C coupling reactions of aldehydes and alcohols can be promoted by monofunctional Cu/SiO_2 catalysts without any detectable assistance by the support. Based on that previous work, it is reasonable to postulate that on our Z$CuSiO_2$ catalysts, the C_2AL and C_3K formation by retroaldol-like reactions involving the C-C bond breaking of the hydroxycarbonyl molecules (HYB and HYA) occurs also on Cu^0 sites, as will be demonstrated below.

We assigned already the direct 1,3-BDO dehydration activity to Cu^0 sites (Scheme 4) based on the results of Fig. 4, but a question remains about what surface site performs the HYB dehydration job that in Scheme 3 was assigned to Cu^0 species. As discussed above, pure silica was inactive for dehydrating or dehydrogenating 1,3-BDO. However, dehydration of aldols, i.e., of

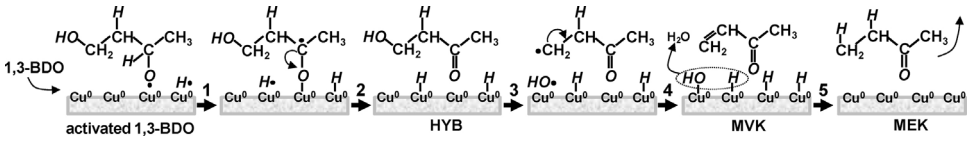

Scheme 3. Surface mechanism for 1,3-BDO conversion via tandem dehydrogenation–dehydration–hydrogenation reactions on ZCuSiO$_2$ catalysts.

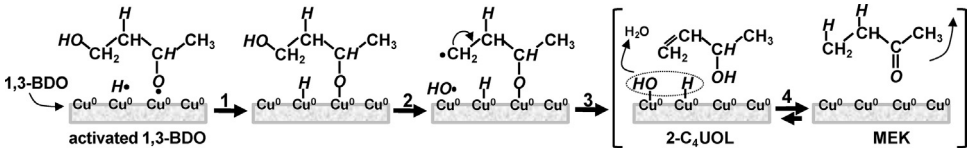

Scheme 4. Surface mechanism for direct 1,3-BDO dehydration to MEK on ZCuSiO$_2$ catalysts.

hydroxycarbonyl compounds (HYB and HYA), is supposed to be less acidity-demanding than that of 1,3-BDO and might take place on the silica sites or on Cu^{n+} sites of ZCuSiO$_2$ samples generated by in situ re-oxidization during the catalytic run. In fact, in a previous work with C_6 aldol compounds, we found that they easily dehydrate giving the α,β-unsaturated carbonyl compound as the main product even on basic catalysts at the high temperatures of the gas phase reaction [49].

Thus, in order to investigate if acidic properties of low copper loading samples could explain their HYB dehydration performance, the acidity of silica silanols and of calcined samples 1.1CuSiO$_2$, 5.6CuSiO$_2$ and 8.5CuSiO$_2$ was probed by FTIR of pyridine, Fig. 6. The reason for these experiments was the fact that for Z values below the Cu^0 monolayer surface coverage probably part of the silica silanols remained unexchanged on the surface after catalyst preparation and they could provide the necessary surface acidity to dehydrate HYB. Results of Fig. 6 indicated that the SiO$_2$ support was not acidic (only H-bonded pyridine bands were observed, [50]) while low Cu content ZCuSiO$_2$ samples showed exclusively the bands typical of pyridine coordinated on Lewis (L) acid sites at 1611 and 1451 cm^{-1} [51]. No band corresponding to pyridinium ion formed on Brønsted (B) acid sites (~1640 and ~1550 cm^{-1}) was observed [51]. Since results showed no measurable Brønsted acidity on these samples we ruled out surface OH groups of low Cu loading ZCuSiO$_2$ samples as responsible for HYB dehydration.

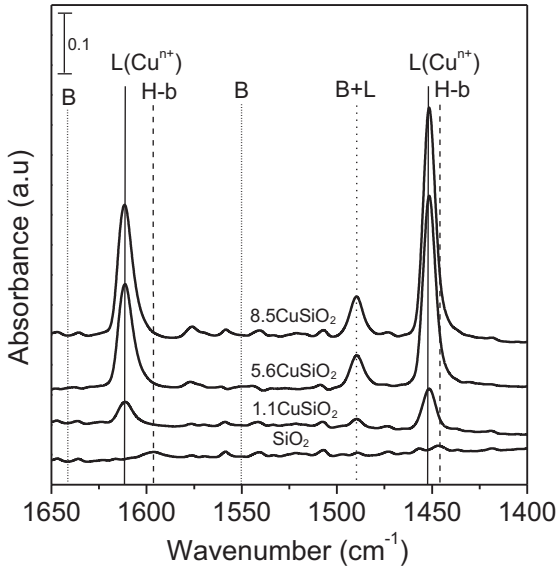

Fig. 6. FTIR spectra after pyridine adsorption at 298 K and evacuation at 423 K on SiO$_2$ and unreduced ZCuSiO$_2$ catalysts. [B: Brønsted; L: Lewis; H-b: H-bonded].

On the other hand, the standard procedure before the catalytic tests included a catalyst reduction at 573 K in flowing hydrogen enough to quantitatively reduce even the low Cu loading ZCuSiO$_2$ samples in which the strong Cu-SiO$_2$ interaction shifts the reduction peak to higher temperatures, as explained above (Fig. 1 and Table 2). Therefore, participation in dehydration steps of Cu^{n+} ions resulting from incomplete catalyst reduction is unlikely. However, surface re-oxidation due to water and other product formation during the catalytic run with in situ generation of weak Cu^{n+} Lewis acid sites cannot be excluded. In fact, the unreduced copper species of low Z samples display Lewis acidic properties, with the intensity of the pyridine adsorption band being proportional to the copper loading, as shown in the FTIR spectra of Fig. 6.

Thus, in order to test the ability of Cu sites for dehydrating HYB, additional catalytic experiments feeding HYB to an empty reactor and to a reactor loaded with SiO$_2$, 2.6CuSiO$_2$, 5.6CuSiO$_2$ and 25.0CuSiO$_2$ were carried out, Table 3. Main reactions during thermal or catalytic HYB conversion were dehydration to MVK and consecutive hydrogenation to MEK, and to a much lesser extent, the C-C bond breaking toward C_3K and other minor compounds and the hydrogenation toward 1,3-BDO, as shown in Scheme 2. The thermal HYB conversion was ~2%. Results showed that SiO$_2$ (entry 1) dehydrates HYB at a low rate, to an extent similar to the thermal reaction. The lack of acidity of the silica silanols suggested by the FTIR results accounts for this finding. On the other hand, on reduced ZCuSiO$_2$ catalysts (entries 2–4) the main reaction pathway for HYB conversion was dehydration, with the unsaturated ketone, MVK, having selectivities higher than 90%. The total HYB conversion (r_{HYB}) and dehydration ($r_{-H_2O} = r_{MVK} + r_{MEK}$) rates were much higher than on SiO$_2$, thereby confirming the participation of Cu sites in HYB dehydration steps on reduced ZCuSiO$_2$ catalysts. However, whether the HYB dehydration occurs on a Cu^0 site or on a re-oxidized Cu^{n+} cation needs still be elucidated. Thus, two additional experiments were carried out with unreduced samples 5.6CuSiO$_2$ and 25.0CuSiO$_2$, entries 5 and 6. Clearly, the performance of fully oxidized copper sites in HYB transformation resembled that of SiO$_2$ (entry 1) in terms of both, total and dehydration activity, and therefore we concluded that weak Lewis acid sites (Cu^{2+}) cannot be responsible for dehydrating HYB at a high rate such as on reduced ZCuSiO$_2$ catalysts (entries 2–4). For the wide Cu compositional range (2.6–25.0 wt.%), the constant values of the HYB turnover rate and of the dehydration, hydrogenation and C-C bond breaking site-time yields indeed confirm that these reactions are promoted by metallic copper sites, Table 3. Thus, Scheme 3, steps 3 and 4, illustrates the homolytic C—OH and C—H bond dissociations on metallic copper sites for HYB dehydration.

The catalytic results for 1,3-BDO and HYB reactions confirm the monofunctional nature of the ZCuSiO$_2$ catalysts and that the sequence of reactions steps participating in dehydrogenation and

Table 3
Reaction data for HYB transformation on reduced and unreduced $ZCuSiO_2$ catalysts.

Entry	Catalyst	r_{HYB}[a] (mol/h gcat) ×100	r_{-H2O}[b] (mol/h gcat) ×100	TOR[c] (1/s) ×100	STY_{-H2O}[d] (1/s) ×100	STY_{C-C}[e] (1/s) ×100	STY_{+H2}[f] (1/s) ×100
1	SiO_2	1.49	1.35	–	–	–	–
2	$2.6CuSiO_2$	3.60	3.28	4.47	4.07	0.36	0.03
3	$5.6CuSiO_2$	5.26	4.62	4.36	3.84	0.50	0.02
4	$25.0CuSiO_2$	4.07	3.79	5.37	4.99	0.36	0.02
5	$5.6CuSiO_2$ (ur)[g]	1.54	1.46	–	–	–	–
6	$25.0CuSiO_2$ (ur)[g]	1.84	1.73	–	–	–	–

T = 523 K; $\bar{P}_{HYB} = 0.9$ kPa; $\bar{P}_{N_2} = 100.4$ kPa.
[a] HYB conversion rate.
[b] Dehydration rate.
[c] Turnover rate in mol HYB/s mol surface Cu.
[d] Site-time yield for dehydration products MVK + MEK.
[e] Site-time yield for C–C bond breaking products $C_1OL + C_2OL + C_2AL + C_3K + 2\text{-}C_3OL$.
[f] Site-time yield for hydrogenation product 1,3-BDO.
[g] Unreduced.

dehydration reactions are promoted on Cu^0 sites. The high number of low-coordination surface Cu^0 species in well dispersed copper particles present in low Z value catalysts tend to dehydrate 1,3-BDO through a fast direct pathway giving mainly the saturated ketone, MEK. On the contrary, at high copper loadings where clustered Cu^0 species are abundant, the 1,3-BDO dehydrogenation to HYB predominates probably because of a weaker HYB–Cu^0 interaction that would allow the HYB molecule to desorb before consecutive dehydration and other reactions take place.

4. Conclusions

Conversion of polyols was studied on copper-silica catalysts prepared by ion exchange technique using 1,3-butanediol as a model molecule. A reaction network for 1,3-butanediol conversion was postulated. It was found that under gas phase conditions 1,3-butanediol can be converted into valuable β-hydroxy, saturated and unsaturated C_4 ketones, and other minor oxygenates by dehydration or by tandem dehydrogenation-dehydration-hydrogenation reactions and to a much lesser extent by C—C bond cleavage reactions. Furthermore, it was found that (de)hydrogenation, dehydration and C—C bond breaking reactions take place on reduced copper sites, the role of silica being to provide a high metal dispersion of low copper content catalysts on which the dehydration selectivity is enhanced. C_4 products were formed in selectivities above 80% thereby confirming that copper metal mostly preserves the C—C bonds of the reactant.

Metal reducibility, dispersion and metal–silica interaction were strongly dependent on the copper loading which also determined the catalyst dehydrogenating or dehydrating properties. Thus, the product distribution could be oriented toward either the β-hydroxy or the saturated ketone by properly tuning copper loading and contact time. On low copper loading (1–12 wt.%) catalysts, the saturated ketone (methyl ethyl ketone) was mainly obtained regardless of the contact time, due to the fast dehydration of both, the reactant and the produced β-hydroxy ketone. Contrarily, at high copper contents (15–25 wt.%) dehydrogenation of the reactant predominates, with the β-hydroxy ketone (4-hydroxy-2-butanone) being obtained as the main product at the contact time range under study.

Acknowledgements

Authors thank the Agencia Nacional de Promoción Científica y Tecnológica (ANPCyT), Argentina (Grant PICT 1888/10), CONICET, Argentina (Grant PIP 11220090100203/10) and Universidad Nacional del Litoral, Santa Fe, Argentina (Grant CAID 51-248/09) for the financial support of this work. They also thank Evonik Industries Argentina and Dr Nicoletta Ravasio for providing the silica sample and Antonio Negro for technical assistance in obtaining the UV–vis–DRS spectra.

References

[1] M.A. Dasari, P.P. Kiatsimkul, W.R. Sutterlin, G.J. Suppes, Appl. Catal. A: Gen. 281 (2005) 225–231.
[2] Encyclopedia Britannica, http://www.britannica.com/EBchecked/topic/236134/glycol, 20 April 2012.
[3] Z.-L. Xiu, A.-P. Zeng, Appl. Microbiol. Biotechnol. 78 (2008) 917–926.
[4] N. Kazuhisa, EP 0787709A1, 1997, to Daicel Chemical Industries Ltd.
[5] K.Windhorst, R.D. Guajardo, WO 068408A1 (2005), to Celanese International Corporation.
[6] Y. Liu, H. Tuysuz, C.-J. Jia, M. Schwickardi, R. Rinaldi, A.-H. Lu, W. Schmidt, F. Schuth, Chem. Commun. 46 (2010) 1238–1240.
[7] R.M. West, E.L. Kunkes, D.A. Simonetti, J.A. Dumesic, Catal. Today 147 (2009) 115–125.
[8] N. Ichikawa, S. Sato, R. Takahashi, T. Sodesawa, K. Inui, J. Mol. Catal. A: Chem. 212 (2004) 197–203.
[9] H.B. Singh, G.E. Klinzing, J. Coull, Ind. Eng. Chem. Prod. Res. Dev. 12 (3) (1973) 184–189.
[10] S. Sato, M. Akiyama, R. Takahashi, T. Hara, K. Inui, M. Yokota, Appl. Catal. A: Gen. 347 (2008) 186–191.
[11] C.-W. Chiu, M.A. Dasari, G.J. Suppes, AIChE J. 52 (10) (2006) 3543–3548.
[12] S. Sato, R. Takahashi, T. Sodesawa, H. Fukuda, T. Sekine, E. Tsukuda, Catal. Commun. 6 (2005) 607–610.
[13] A.V. Grishchenko, A.V. Devekii, V.S. Fedorov, N.F. Grishchenko, J. Appl. Chem. USSR 57 (1984) 2365–2368.
[14] S. Sato, R. Takahashi, H. Fukuda, K. Inui, J. Mol. Catal. A: Chem. 272 (2007) 164–168.
[15] A. Corma, G.W. Huber, L. Sauvanaud, P. O'Connor, J. Catal. 257 (2008) 163–171.
[16] N. Ichikawa, S. Sato, R. Takahashi, T. Sodesawa, J. Mol. Catal. A: Chem. 256 (2006) 106–112.
[17] T. Mukaiyama, Org. React. 28 (1982) 203–331.
[18] H. Zhang, G.T. Lountos, C.B. Ching, R. Jiang, Appl. Microbiol. Biotechnol. 88 (2010) 117–124.
[19] Y. Su, Y.-M. Liu, L.-C. Wang, M. Chen, Y. Cao, W.-L. Dai, H.-Y. He, K.-N. Fan, Appl. Catal. A: Gen. 315 (2006) 91–100.
[20] N. Ichikawa, S. Sato, R. Takahashi, T. Sodesawa, Catal. Commun. 6 (2005) 19–22.
[21] L. Wang, H. Zhang, C.-B. Ching, Y. Chen, R. Jiang, Appl. Microbiol. Biotechnol, Online, http://dx.doi.org/10.1007/s00253-011-3699-z, 2011.
[22] T. Iwahama, Y. Yoshino, T. Keitoku, S. Sakaguchi, Y. Ishii, J. Org. Chem. 65 (2000) 6502–6507.
[23] J.I. Di Cosimo, G. Torres, C.R. Apesteguía, J. Catal. 208 (2002) 114–123.
[24] F. Boccuzzi, S. Coluccia, G. Martra, N. Ravasio, J. Catal. 184 (1999) 316–326.
[25] V. Di Castro, M. Gargano, N. Ravasio, M. Rossi, in: G. Poncelet, P.A. Jacobs, P. Grange, B. Delmon (Eds.), Studies in Surface Science and Catalysis, vol. 63, Elsevier, Amsterdam, 1991, p. 95.
[26] A. Gervasini, S. Bennici, Appl. Catal. A: Gen. 281 (2005) 199–205.
[27] E.D. Guerreiro, O.F. Gorriz, J.B. Rivarola, L.A. Arrúa, Appl. Catal. A: Gen. 165 (1997) 259–271.
[28] G.C. Bond, S.N. Namijo, J. Catal. 118 (1989) 507–510.
[29] F.-W. Chang, H.-C. Yang, L.S. Roselin, W.-Y. Kuo, Appl. Catal. A: Gen. 304 (2006) 30–39.
[30] F.M. Mirabella, Modern Techniques in Applied Molecular Spectroscopy, first ed., Wiley-Interscience, New York, 1998.
[31] L. Trouillet, T. Toupance, F. Villain, C. Louis, Phys. Chem. Chem. Phys. 2 (2000) 2005–2014.
[32] M. Shimokawabe, N. Takezawa, H. Kobayashi, Appl. Catal. A: Gen. 2 (1982) 379–387.
[33] J.D. Le Grange, J.L. Markham, C.R. Kurkjian, Langmuir 9 (1993) 1749–1763.
[34] T. Toupance, M. Kermarec, J.-F. Lambert, C. Louis, J. Phys. Chem. B 106 (2002) 2277–2286.

[35] M. Popova, M. Dimitrov, V. Dal Santo, N. Ravasio, N. Scotti, Catal. Commun. 17 (2012) 150–153.
[36] J.I. Di Cosimo, C.R. Apesteguía, J. Mol. Catal. 91 (1994) 369–386.
[37] G. Fierro, M. Lo Jacono, M. Inversi, P. Porta, F. Cioci, R. Lavecchia, Appl. Catal. A: Gen. 137 (1996) 327–348.
[38] D. An, Q. Zhang, Y. Wang, Catal. Today 157 (2010) 143–148.
[39] M. Karthik, L.-Y. Lin, H. Bai, Microporous Mesoporous Mater. 117 (2009) 153–160.
[40] S. Velu, K. Suzuki, M. Okazaki, M.P. Kapoor, T. Osaki, F. Ohashi, J. Catal. 194 (2000) 373–384.
[41] C.F. de Graauw, J.A. Peters, H. van Bekkum, J. Huskens, Synthesis (1994) 1007–1017.
[42] J.I. Di Cosimo, A. Acosta, C.R. Apesteguía, J. Mol. Catal. A: Chem. 234 (2005) 111–120.
[43] R.T. Morrison, R.N. Boyd, Organic Chemistry, sixth ed., New York University, Prentice Hall of India Private Limited, New Delhi, 2002.
[44] M.A. Kohler, H.E. Curry-Hyde, A.E. Hughes, B.A. Sexton, N.W. Cant, J. Catal. 108 (1987) 323–333.
[45] A. Bienholz, H. Hofmann, P. Claus, Appl. Catal. A: Gen. 391 (2011) 153–157.
[46] M.G. Musolino, P. De Maio, A. Donato, R. Pierpaolo, J. Mol. Catal. A: Chem. 208 (2004) 219–224.
[47] J.I. Di Cosimo, A. Acosta, C.R. Apesteguía, J. Mol. Catal. A: Chem. 222 (2004) 87–96.
[48] M.E. Sad, M. Neurock, E. Iglesia, J. Am. Chem. Soc. 133 (50) (2011) 20384–20398.
[49] J.I. Di Cosimo, V.K. Díez, C.R. Apesteguía, Appl. Catal. A: Gen. 137 (1996) 149–166.
[50] V.V. Ordomsky, V.L. Sushkevich, I.I. Ivanova, J. Mol. Catal. A: Chem. 333 (2010) 85–93.
[51] M.M. Mohamed, E.F. Vansant, Colloid Surf. A: Physicochem. Eng. Aspects 96 (1995) 253–260.